Journal of Power Sources 227 (2013) 171–176

Contents lists available at SciVerse ScienceDirect

Journal of Power Sources

journal homepage: www.elsevier.com/locate/jpowsour

A coupled nonlinear equivalent circuit – Thermal model for lithium ion cells

Krishnan S. Hariharan*

India Science Lab, General Motors Global R&D, Creator Building, International Technology Park, Whitefield Road, Bangalore 560066, India

HIGHLIGHTS

- ► Nonlinear equivalent circuit model with energy balance for lithium ion cells.
- ► Temperature-dependent variable resistors.
- ► The cell voltage and temperature represented by one pair RC model.
- ► Rate of heat generation steeply rises near the end of discharge.
- ► Coolant with higher heat transfer coefficient result in lower operating efficiency.

ARTICLE INFO

Article history:
Received 3 October 2012
Received in revised form
13 November 2012
Accepted 15 November 2012
Available online 23 November 2012

Keywords:
Lithium ion battery
Nonlinear equivalent circuit model
Temperature based variable resistances
Battery management system

ABSTRACT

A nonlinear equivalent circuit model is developed for lithium ion cells using variable resistors that are functions of the cell temperature. The voltage and thermal characteristics of a commercial cell with a $LiFePO_4$ positive and graphite negative electrode are modeled using a lumped energy balance coupled with the equivalent circuit representation. The cell voltage and temperature during full depth charge–discharge operations can be represented accurately by a one pair RC model. The model is able to represent cell voltage and temperature over a wide range of powers with a global set of parameters. The parameters established, model predictions of the heat generation rates under various conditions are examined. Due to the unique discharge behavior of $LiFePO_4$ positive electrode, the rate of heat generation is constant over most of the state of charge (*SOC*) window and steeply rises near the end of discharge. A higher heat transfer coefficient of the cooling medium, in addition to lowering the operating voltage, results in higher heat generation. Thus battery cooling systems should be designed to operate at an optimal rate of heat removal considering the operating efficiency, in addition to battery life.

1. Introduction

The lithium ion battery technology is established as the primary energy source in electric vehicle or hybrid electric vehicle applications due to its high energy density, light weight, low self-discharge and other features [1]. At present, a phospho-olivine compound, lithium iron phosphate ($LiFePO_4$) [2], has proven to be one of the leading candidates as the positive electrode material for hybrid and electric vehicle applications. $LiFePO_4$ is environmentally benign, highly stable, and inexpensive with a high capacity and operating voltage. A pertinent problem that has been observed in lithium based batteries is that of thermal runaway. Especially for large scale applications like automobiles, where a large array of cells are connected together, thermal management becomes critical and presently is one of the singular challenges for the industrial utilization of lithium based cells.

During battery discharge/charge, various electrical and electrochemical processes take place that release heat. Thermal modeling is an efficient way to calculate the temperature rise during operation and develop various cooling schemes for batteries. Thermal modeling gives insights into the contributions of the individual electrochemical processes. The general energy balance approach developed around two decades ago [3] has been incorporated in the macroscale continuous models [4] to calculate the temperature changes [5] during battery operations. Other developments in this area include two- and three-dimensional thermal models [6,7], finite element models [8] and models for EV batteries [9]. Electrochemical thermal [10] models that examine the interactions between electrochemical and thermal processes, approaches in modeling of $LiCoO_2$ based batteries [11] and recent developments on distributed thermal models [12] are worth

* Present address: Samsung Advanced Institute of Technology-India, SISO Pvt. Ltd., Bangalore 560093, India. Tel.: +91 80 4201 2749; fax: +91 80 4115 8262.
E-mail address: krishnan.sh@gmail.com.

0378-7753/$ – see front matter © 2012 Elsevier B.V. All rights reserved.
http://dx.doi.org/10.1016/j.jpowsour.2012.11.044

mentioning in this context. Under normal conditions cell thermal response is modeled [13] using lumped parameters and heat generation rates as well.

Equivalent circuit models where the voltage response of the cell is represented as an electric circuit [14] has received much importance due to conceptual simplicity and applicability. These models can be integrated with control algorithms at a system level for on-board applications in an automobile. To develop an accurate model for battery performance, equivalent circuit models require less amount of data, must be robust, accurate over a wide range of operating conditions and easy to compute. The pertinent variables do not have spatial dependence and the model equations based on electrical circuit theory are solved as a set of ordinary differential equations. The equivalent circuit model is coupled with the energy balance models [15] to characterize the thermal behavior of NiMH battery packs with sufficient accuracy. The entropy of the $LiFePO_4$–graphite cell is measured [16] and the thermal characteristics are represented as a thermal equivalent circuit.

In a recent work [17], a nonlinear equivalent circuit model is developed using over-potential based variable resistors. The model is able to accurately represent the pulse voltage response of commercial lithium ion cells. This model, however, is developed for isothermal conditions. During cell operations, there is substantial amount of heat release and a non-isothermal model is essential to study the thermal response under these conditions. A non-isothermal model can be used to understand the dependence of the rate of heat generation on operating conditions and minimize thermal losses. In the present work a non-isothermal nonlinear equivalent circuit is developed using variable resistors that are functions of cell temperature. The equivalent circuit model is solved with the energy balance equation to obtain cell voltage and temperature simultaneously. The coupled model is used to study voltage and thermal characteristics of a commercial cell with $LiFePO_4$ positive and graphite negative electrode. In the previous work [17] the parameters are estimated from isothermal HPPC (Hybrid Pulse Power Characterization) data with minimal temperature variations during the pulse. As the aim of the present work is to develop a non-isothermal model, the parameters are estimated from a full depth discharge–charge data at various temperatures. As voltage and temperature are obtained simultaneously, the present approach can be potentially used as an on-board state estimator in battery management systems.

In the first part of study, parameters are estimated by minimizing the error between model outputs and experimental data. The global set of parameters thus estimated, model predictions of heat generation rates under various conditions are examined. In order to conceive appropriate cooling concepts when cells are used as energy source in automobiles, it is important to understand the dependence of heat generation on operating conditions. The interaction of the cell with the battery cooling system is through the heat transfer coefficient. Hence in the subsequent section, the effect of heat transfer coefficient on cell temperature and rate of heat generation is studied in detail. The results of this study provide key insights in the design of an efficient battery thermal management system.

2. Model development and experimental data

In the equivalent circuit approach various electrochemical processes in the cell are represented in terms of equivalent resistors, capacitors or other electric circuit elements. The general representation for a cell, with processes identified using electrochemical impedance spectroscopy (EIS) [18] is that of a sequence of RC (R is parallel to C) circuits with a Warburg element for diffusion. An equivalent representation amenable for time domain analysis is that of an N pair RC [17]. Output of an electric circuit model is the cell voltage represented in terms of cell current, equilibrium potential and the model parameters. Effect of temperature on individual electrochemical processes enters the equivalent circuit model through the temperature dependence of model parameters. Cell temperature is obtained using a lumped energy balance once cell voltage, entropy of charge transfer reaction and heat transfer coefficient of the cooling medium are known. By coupling the equivalent circuit and lumped energy balance models, cell voltage and temperature are obtained under any operating conditions. Details of the equivalent circuit model and the lumped energy balance are described in the next section. The subsequent section discusses the experimental data used in the model.

2.1. The equivalent circuit model and energy balance

In absence of degradation, important processes in a cell are ionic and electronic conduction, charge transfer reaction and lithium diffusion in the electrodes. In a recent work [17], it is shown that pulse response of a lithium ion cell is accurately represented by a 2 pair RC circuit. In the present work the interest is on modeling full depth charge–discharge processes and further simplifications to the model are sought. For example, it can be expected that faster transients, represented by one of the RC pairs are not significant. The resultant equivalent circuit is a 1 pair RC model (Fig. 1), and hence is considered in this study. The 1 pair RC model has a high frequency resistor R and a low frequency resistor R_{ct} parallel to a capacitor C. The high frequency resistor R represents ionic and electronic conduction, capacitor C represents the double layer and all the transients and resistor R_{ct} represents resistance due to all transport processes – diffusion in the electrodes and charge transfer reaction. It should be noted that in this level of representation, distinction between the electrodes is not made. The 1 pair RC model, though simplistic, has been successful in representing [14] the charge–discharge characteristics of lithium ion cells. The principal equation governing the cell behavior is the voltage balance across the cell:

$$V = V_0 + IR + V_1 \tag{1}$$

In Eq. (1), cell voltage V is related to equilibrium potential V_0, voltage drop across the resistance R due to current I, and voltage drop across the RC pair (R_{ct} parallel to C), V_1. The current balance across the RC pair is:

$$I = I_C + I_{R_{ct}}, \tag{2}$$

Eq. (2) can be rewritten in terms of capacitance C and resistance R_{ct} as

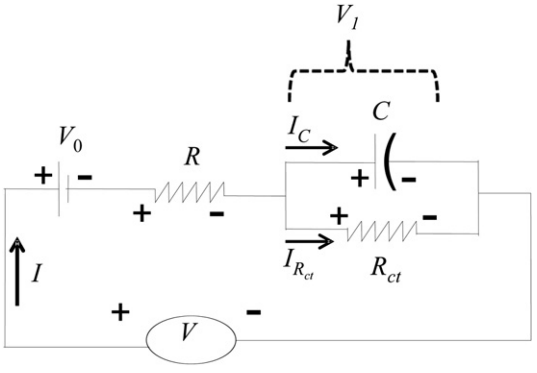

Fig. 1. The 1 pair RC equivalent circuit model.

$$I = \frac{\mathrm{d}}{\mathrm{d}t}[CV_1] + \frac{V_1}{R_{ct}}. \quad (3)$$

Thus Eqs. (1) and (3) are solved to obtain the cell voltage for at any current, once R, R_{ct} and C and equilibrium potential V_0 are known. V_0 is a function of the cell state of charge (SOC) and is estimated from the current history as defined below:

$$SOC = SOC_0 + \frac{1}{Q_{max}} \int_o^t I\mathrm{d}t \quad (4)$$

where Q_{max} is the maximum columbic capacity of the cell, and SOC_0 corresponds to the initial SOC. The equilibrium relationship between V_0 and the state of charge (SOC) is typically known from HPPC experiments. The initial value of V_1 is obtained by solving Eq. (1) at time $t = 0$.

The nonlinear equivalent circuit in this study is constructed using temperature-dependent variable resistors. In an equivalent circuit framework, assigning of temperature dependence for individual electrochemical processes is done through EIS [19]. For $LiFePO_4$ based electrodes, the temperature dependence of charge transfer resistances and lithium diffusion in the electrodes have been reported to have Arrhenius dependence [20]. Hence the model resistances are represented by the functions as shown:

$$R = R_0 e^{E/R_g T} \quad (5)$$

$$R_{ct} = R_{ct0} e^{E_{ct}/R_g T} \quad (6)$$

In Eqs. (5) and (6), E and E_{ct} are the activity coefficients and R_g the gas constant and T the temperature, in K. The parameters of the equivalent circuit model are $\{R_0, R_{ct0}, E \text{ and } E_{ct}\}$.

The energy balance [3] for a cell in the lumped parameter framework is given by [15]:

$$MC_P \frac{\mathrm{d}T}{\mathrm{d}t} = I(V - V_0) + IT\frac{\mathrm{d}V_0}{\mathrm{d}T} + hA(T_A - T) \quad (7)$$

In Eq. (7), T is the surface temperature of the cell, M the mass, C_P the specific heat, h the heat transfer coefficient of the cooling medium, and A the outer surface area of the cell available for heat transfer. In the lumped parameter approach, temperature variations within the cell are not accounted for. Eq. (7) accounts for increase in cell temperature due to heat generation within the cell and heat transfer to the ambient by convection. The first term on the right hand side of Eq. (7) is the irreversible heat generation due to passage of current I resulting from an over-potential, $V–V_0$. The second term is the reversible heating and is related to the entropy of the charge transfer reaction. The third term corresponds to the heat transferred to the ambient at temperature T_A, with a heat transfer coefficient h.

2.2. Experimental data

Commercial cells with lithium iron phosphate ($LiFePO_4$) positive and a graphitic carbon negative have been used in this study. Spirally wound cylindrical cells of 26 mm diameter and 65 mm length weighed 0.074 kg with the tabs. The nominal voltage is 3.3 V and the nominal capacity is 2.3 amp-hours (Ah). The experimental data used in this study are constant power full depth discharge and charge at 45 °C, 25 °C and 0 °C. At 45° and 25 °C, discharge powers ranging from 3 W to 75 W and charge powers ranging from 3 W to 30 W are considered, and the highest power at 0 °C is 20 W. The equilibrium potential V_0 is obtained from HPPC experiments conducted at various temperatures. Temperature is measured at the surface of the cells. The atmospheric chamber has fans for air circulation to enable convection and eventual cooling of the cells. In a recent work [16] the $\mathrm{d}V_0/\mathrm{d}T$ of similar type of cells is reported in the temperature range of 6 °C–36 °C, and are used in this study.

3. Results and discussions

3.1. Voltage and thermal characterization

The voltage response of the model is obtained by solving Eqs. (1) and (3), with the temperature dependence of the resistors given by Eqs. (5) and (6). The cell temperature is obtained by solving Eq. (7) that couples with Eq. (1) for cell voltage. The unknown parameters are R_0, E, R_{ct0}, E_{ct} and C for the equivalent circuit model (Eqs. (1) and (3)) and h, C_p for the energy balance (Eq. (7)). In order to reduce the number of unknown parameters in the energy balance equation, it is observed that at zero current Eq. (7) reduces to

$$MC_P \frac{\mathrm{d}T}{\mathrm{d}t} = hA(T_A - T) \quad (8)$$

In Eq. (8), T corresponds to the cell surface temperature and A the surface area of the cylindrical cells. Eq. (8) is easily solved to give

$$T = T_A + ae^{-\frac{hA}{MC_P}t} \quad (9)$$

Thus the ratio, h/C_p can be obtained from fitting Eq. (9) to the experimental temperatures when no current is passed. An average value of this ratio over all ambient temperatures is estimated to be 0.0175 with ±10% standard deviation. This ratio is used in Eq. (7) to express C_p in terms of h. Other 6 parameters of the model, R_0, E, R_{ct0}, E_{ct}, C and h are extracted by minimizing the error between the model output and measured values of voltage and temperature. A global set of parameters that represent the complete charge and discharge behavior is obtained by minimizing the root mean square error (RMSE) between the model output and the experimental voltage at all powers and temperatures. The RMSE is defined by:

$$\mathrm{RMSE} = \sqrt{\frac{1}{N}\sum_{j-1}^{N}(1 - V_{model}/V_{exp})^2 + (1 - T_{model}/T_{exp})^2}, \quad (10)$$

The global parameters obtained by this exercise are shown in Table 1.

The comparison of the model and experimental voltage for discharge as well as charge operation at 45 °C is shown in Fig. 2. In order to represent data at all the powers in the same scale, the voltage is plotted against time multiplied by the respective absolute powers of operation. It can be seen from Fig. 2 that the model represents the discharge voltage fairly accurately at all times at 3 W, 25 W and 50 W. At the highest power (75 W), the model has a constant discharge voltage for a longer period of time in comparison with the experiments. The charge voltages at all

Table 1
Global parameters of the model.

Parameter	Value
R_0	6.7169e−007 Ω
E/R_g	2966.1 K
R_{ct0}	4.3323e−006 Ω
E_{ct}/R_g	2480.6 K
C	4725.1 F
h	29.867 W m^{-2} K^{-1}
C_P	1699.1 J kg^{-1} K^{-1}

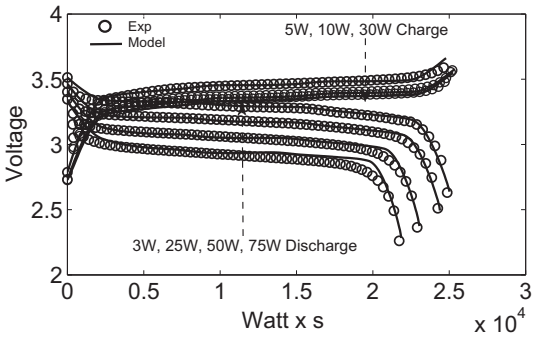

Fig. 2. Comparison between experimental and model voltage during discharge and charge at 45 °C for the various powers indicated in the figure.

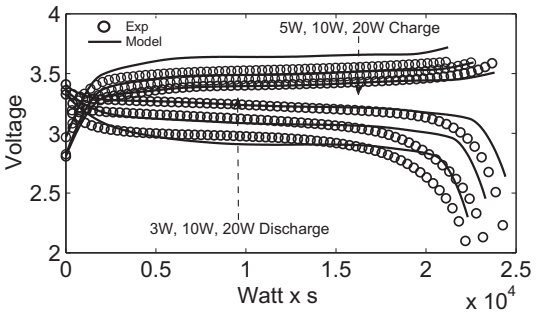

Fig. 4. Comparison between experimental and model voltage during discharge and charge at 0 °C for the various powers indicated in the figure.

powers and at all times are accurately represented by the model. The results at 25 °C are shown in Fig. 3. The trends in the discharge voltage are similar to Fig. 2 although there is some mismatch during intermediate times of discharge. The drop in the voltage near the end of discharge is accurately represented by the model. The charge voltages except at 30 W are also captured well. At the lowest temperature (0 °C, Fig. 4) although the model discharge and charge voltages are close to the experimental data for powers till 10 W, the model consistently over estimates the discharge capacity.

The comparison between the model and measured temperatures for discharge data at all ambient temperatures at various powers is shown in Fig. 5. It can be observed that the temperature rise at 75 W at 25 °C is higher than at 45 °C for the same power. This is probably because the resistances are higher at lower temperatures, leading to higher rates of heat generation. The model adequately represents the temperature rise at all temperatures although there is a slight mismatch near the end of discharge at 0 °C. The corresponding results for the charge data are shown in Fig. 6. The model compares well with the measured temperatures at all powers at 45 °C and at 5 and 10 W at the other temperatures. The temperature profiles at the highest power are over estimated by the model at 25 as well as 0 °C. The mismatch for the temperature (Figs. 5 and 6) as well as the voltage profiles (Fig. 4) at 0 °C could be due to the fact the experimental dV_0/dT values are available only till 6 °C. Given this level of comparison, it is to be noted that the only parameter in the energy balance equation (Eq. (7)) extracted from the experimental data is the heat transfer coefficient.

This section can be concluded by stating that a 1 pair RC model is able to represent the cell voltage and temperature at various powers and ambient temperatures with a global set of parameters. The equivalent circuit model is constructed with temperature dependent variable resistors. During any cell operation, the temperature continuously changes and according to Eqs. (5) and (6), the resistances of the model, R and R_{ct} vary continuously to capture the voltage characteristics of the cell. As the temperature is obtained by solving the coupled energy balance the combined model can be used to represent the cell behavior in a consistent manner. It is to be noted that the *SOC* changes continuously during a full depth process. However the model parameters do not need an explicit dependence on *SOC* to represent the cell voltage and temperature for the range of data analyzed in this work.

3.2. Rate of heat generation and effect of heat transfer coefficient

During a cell discharge/charge, there is irreversible as well as reversible generation of heat (Eq. (7)). The former is expressed in terms of the over-potential $V-V_0$, and the latter in terms of the entropy of the charge transfer reaction. The total rate of heat generation is the sum of the two contributions. The total rate of heat generation computed from measured voltage and temperature at various powers using Eq. (7) for discharge at 25 °C is shown in Fig. 7 along with the model predictions. The latter uses voltage and temperature computed from the model. It can be seen that heat generation increases with the power and the model is able to predict the trends in total rate of heat generation at all powers studied.

It can be seen from Fig. 7 that rate of heat generation is almost constant between *SOC*s of 0.8 and 0.2 and increases substantially near the end of discharge. Cells with $LiFePO_4$ as the positive electrode have a constant output voltage at these *SOC*s due to the multiphase coexistence observed in the material [2]. This output voltage

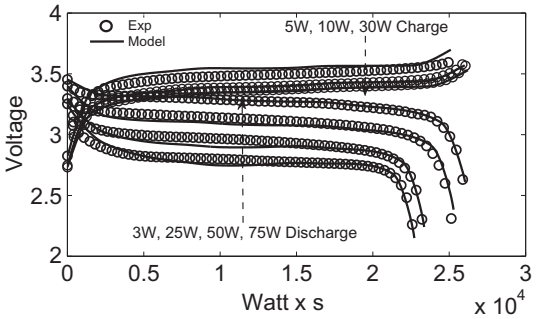

Fig. 3. Comparison between experimental and model voltage during discharge and charge at 25 °C for the various powers indicated in the figure.

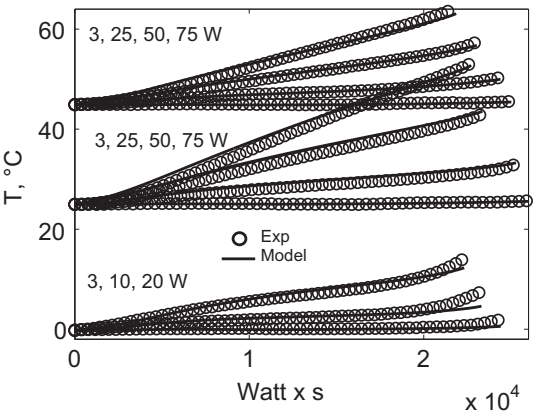

Fig. 5. Comparison between experimental and model temperatures during discharge at 45 °C, 25 °C and 0 °C and the various powers indicated in the figure.

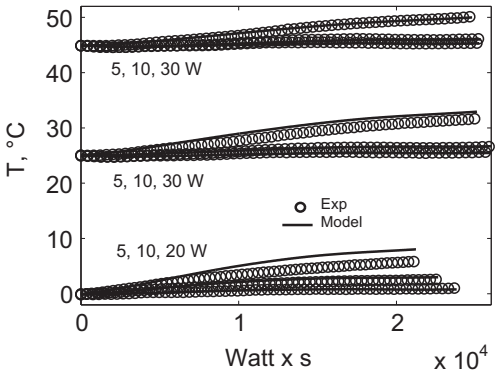

Fig. 6. Comparison between experimental and model temperatures during charge at 45 °C, 25 °C and 0 °C and the various powers indicated in the figure.

results in a constant over-potential and in a constant value of the irreversible component of the total heat generated (Eq. (7)). The rapid decrease in cell voltage and the corresponding increase in rate of heat generation near the end of discharge occur either due to emptying of the negative electrode or ending of multi-phase coexistence in the positive electrode [21]. This feature of $LiFePO_4$ based cells can be utilized to minimize the heat losses while operation by choosing a suitable *SOC* window that avoids rapid rise in heat generation.

The sensitivity of the thermal behavior of the cell to heat transfer coefficient is discussed subsequently. This exercise, although done at a single cell level, is aimed to provide insights about the method of cooling to be adapted to minimize heat losses. It would be also important to see if any of the cooling methods would result in undesirable temperatures where the cell to could be potentially damaged. Hence, the results are analyzed at highest temperature and power. The model prediction of cell temperature rise at 45 °C and 75 W is shown in Fig. 8 for various cooling scenarios mentioned in the figure, characterized by heat transfer coefficients [22], corresponding to $h = 0$, 3, 10, 29.87, 60,100, 200 and 1000 W m^{-2} K^{-1} respectively. The measured temperature at 45 °C and 75 W is also shown for comparison. As expected, the temperature rise is higher at lower values of heat transfer coefficient. The corresponding model prediction of the total rates of heat generation (sum of irreversible and reversible components, Eq. (7)) at the same values of '*h*' are shown in Fig. 9, and it can be observed

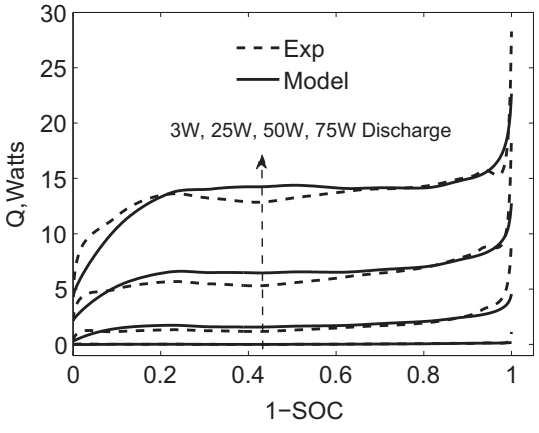

Fig. 7. Comparison of model prediction of total heat generation and the values computed using measured voltage and temperatures (denoted as 'Exp') at various powers indicated in the figure at 25 °C.

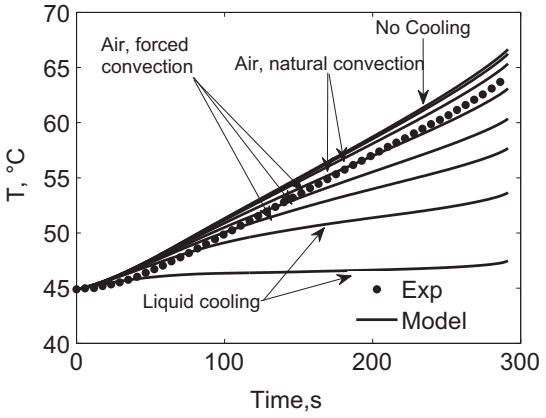

Fig. 8. Dependence of the temperature rise during discharge on heat transfer coefficient at 75 W and 45 °C. The heat transfer coefficients corresponding to the various cooling scenarios shown in figure are $h = 0$, 3, 10, 29.87, 60,100, 200 and 1000 W m^{-2} K^{-1} respectively. The temperature rise is higher at lower values of the heat transfer coefficient.

that the rate of heat generation increases as the heat transfer coefficient is increased. Thus the temperature rise is the highest when the cell is insulated ($h = 0$ W m^{-2} K^{-1}) and the rate of heat generation is highest at a very high value of the heat transfer coefficient ($h = 1000$ W m^{-2} K^{-1}).

This feature can be explained by the corresponding model predictions of the discharge voltages as shown in Fig. 10. It can be seen that the discharge voltage is lower at higher heat transfer coefficients. This is because of lower temperatures at high values of '*h*' (Fig. 8) and consequently higher values of resistances (Eqs. (5) and (6)). A lower voltage leads to a higher magnitude of over-potential ($V–V_0$) and eventually a higher rate of irreversible heat generation, the predominant contribution at high rates [8] of discharge. This observation is of immediate relevance to design of battery cooling systems in automobiles. It is desirable to have a cooling system with a higher heat transfer coefficient to reduce the cell temperatures, as higher temperatures reduce battery life. However under these conditions, higher amounts of the electrical energy taken in by the cell while charging are wasted as irreversible heat and are not available as electrical energy during discharge. Thus a high value of the heat transfer coefficient, in addition to a lower operating voltage results in higher heat generation, and a low value results in higher temperatures affecting battery life. An appropriate cooling system should be designed with an optimal

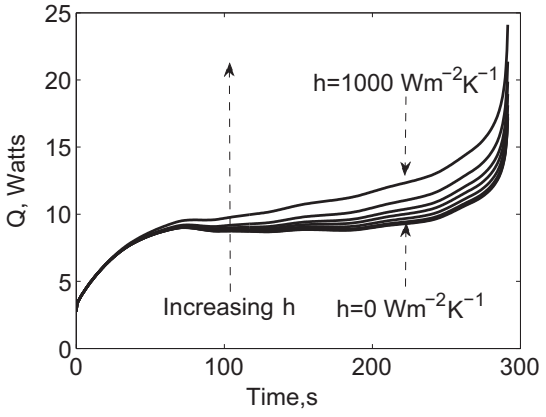

Fig. 9. Dependence of the total rate of heat generation on heat transfer coefficient. Rate of heat generation increases as the heat transfer coefficient is increased.

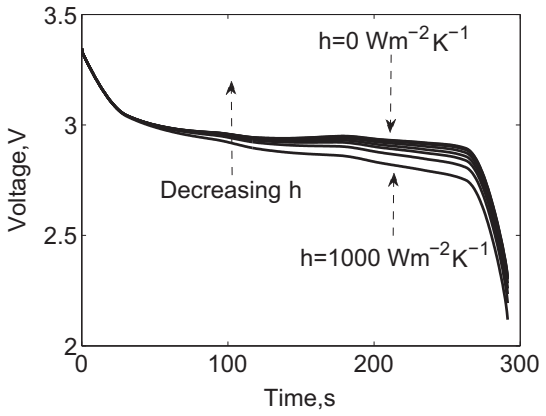

Fig. 10. The discharge voltages at values of heat transfer coefficient corresponding to Fig. 8.

heat transfer coefficient considering the operating efficiency as well as battery life.

4. Summary and conclusions

The voltage and thermal characteristics of a commercial lithium ion cell consisting of $LiFePO_4$ positive electrode and graphite negative electrode are modeled using an energy balance coupled with a nonlinear equivalent circuit representation. The nonlinear equivalent circuit model is constructed using variable resistors that are functions of cell temperature. The cell voltage and temperature during full depth operation during discharge and charge can be represented very accurately by a 1 pair RC model. The model is able to represent the discharge voltage at powers ranging from 3 W to 75 W and charge voltage at powers ranging from 5 W to 30 W and temperatures ranging from 45 °C to 0 °C with a global set of parameters. Although the parameters do not vary during the cell operations, the resistances of the model R and R_{ct} change continuously with temperature to capture the voltage characteristics of the cell. As the temperature and voltage are obtained simultaneously, the combined model can be potentially used as on-board state estimators in battery management systems. Once the global set of parameters is estimated from experimental data, model predictions of the heat generation rates under various conditions are examined. The rate of heat generation is constant for a wide range of *SOC* and steeply rises near the end of discharge. This indicates that the thermal losses can be minimized by choosing a suitable *SOC* window of operation. The temperature profiles and rates of heat generation are studied at various heat transfer coefficients that correspond to different cooling scenarios. A low value of the heat transfer coefficient results in higher temperatures, potentially affecting battery life. However a high value of heat transfer coefficient results in lower operating voltage and higher heat generation. Thus battery cooling systems should be designed to operate at an optimal rate of heat removal considering the operating efficiency, in addition to battery life.

Acknowledgments

The author wishes to acknowledge Mark W. Verbrugge (Global General Motors R&D) for the technical inputs, Ramona. Y. Ying (Global General Motors R&D) for the charge discharge data of the commercial cells and V. Senthil Kumar for insightful discussions.

References

[1] J.-M. Tarascon, M. Armand, Nature 414 (2001) 35.
[2] A.K. Padhi, K.S. Nanjundaswamy, J.B. Goodenough, J. Electrochem. Soc. 144 (1997) 1188.
[3] D. Bernardi, E. Pawlikowski, J. Newman, J. Electrochem. Soc. 132 (1985) 5.
[4] M. Doyle, T.F. Fuller, J. Newman, J. Electrochem. Soc. 140 (1993) 1526.
[5] C.R. Pals, J. Newman, J. Electrochem. Soc. 142 (1995) 3274–3282.
[6] Y. Chen, J.W. Evans, J. Electrochem. Soc. 143 (1996) 2708.
[7] Y. Inui, Y. Kobayashi, Y. Watanabe, Y. Watase, Y. Kitamura, Energy Convers. Manage. 48 (2007) 2103.
[8] D.H. Jeon, S.M. Baek, Energy Convers. Manage. 52 (2011) 2973.
[9] J. Lee, K.W. Choi, N.P. Yoo, C.C. Christianson, J. Electrochem. Soc. 133 (1986) 1286.
[10] L. Song, J.W. Evans, J. Electrochem. Soc. 147 (2000) 2086.
[11] K. Kumaresan, G. Sikha, R.E. White, J. Electrochem. Soc. 155 (2008) A164.
[12] M. Guo, R.E. White, J. Power Sources 221 (2013) 334.
[13] S. Al Hallaj, H. Maleki, J.S. Hong, J.R. Selman, J. Power Sources 83 (1999) 1.
[14] M.W. Verbrugge, R.Y. Ying, J. Electrochem. Soc. 154 (2007) A949.
[15] M.W. Verbrugge, R.S. Conell, J. Electrochem. Soc. 149 (2002) A45.
[16] C. Forgez, D.V. Do, G. Friedrich, M. Morcrette, C. Delacourt, J. Power Sources 195 (2010) 2961.
[17] K.S. Hariharan, V. Senthil Kumar, J. Power Sources 222 (2013) 210.
[18] E. Barsoukov, J.R. MacDonald (Eds.), Impedance Spectroscopy – Theory, Experiment and Applications, second ed., John Wiley and Sons, New Jersey, 2006.
[19] A.J. Bard, L.R. Faulkner, Electrochemical Methods, Wiley, New York, 2001.
[20] M. Takahashi, S. Tobishima, K. Takei, Y. Sakurai, Solid State Ionics 148 (2002) 283.
[21] V. Srinivasan, J. Newman, J. Electrochem. Soc. 151 (2004) A1530.
[22] C.J. Geankoplis, Transport Processes and Unit Operations, PHI, New Delhi, 1997.

Nomenclature

SOC: cell state of charge
V_0: cell equilibrium potential, V
V: cell voltage, V
I: cell current, A
V_1: voltage drop across *RC* pair, V
R_{ct}: resistance representing the charge transfer reaction and diffusion, Ω
R: resistance representing the electronic/ionic conductivity, Ω
C: capacitance representing the double layer and other transients, F
Q_{max}: maximum columbic capacity of the cell, Ah
M: mass of the cell, kg
C_P: specific heat capacity, J kg^{-1} K^{-1}
h: heat transfer coefficient, W m^{-2} K^{-1}
Q: rate of heat generation, W
F: Faradays constant, 96,485 C mol^{-1}